Atmos. Chem. Phys. Discuss., 8, 19743–19789, 2008
www.atmos-chem-phys-discuss.net/8/19743/2008/

Atmospheric Chemistry and Physics Discussions

This discussion paper is/has been under review for the journal *Atmospheric Chemistry and Physics (ACP)*. Please refer to the corresponding final paper in *ACP* if available.

Synoptic influences on springtime tropospheric O_3 and CO over the North American export region observed by TES

J. Hegarty, H. Mao, and R. Talbot

Institute for the Study of Earth, Oceans and Space, Climate Change Research Center, University of New Hampshire, Durham, New Hampshire 03824, USA

Received: 27 August 2008 – Accepted: 24 September 2008 – Published: 19 November 2008

Correspondence to: J. Hegarty (jhegarty@ccrc.sr.unh.edu)

Published by Copernicus Publications on behalf of the European Geosciences Union.

Abstract

The relationship between synoptic circulation patterns over the western North Atlantic Ocean in spring (March, April, and May) and tropospheric O_3 and CO was investigated using retrievals from the Tropospheric Emission Spectrometer (TES) for 2005 and 2006. Seasonal composites of TES retrievals reprocessed to remove the artificial geographic structure added from the a priori revealed a channel of slightly elevated O_3 (>55 ppbv) and CO (>115 ppbv) at the 681 hPa retrieval level between 30° N and 45° N extending from North America out over the Atlantic Ocean. Ozone and CO in this region were correlated at r=0.32 with a slope value of 0.16 indicative of the overall impact of photochemical chemical processes in North American continental export. Composites of TES retrievals for the six predominant circulation patterns identified as map types from sea level pressure fields of the NCEP FNL analyses showed large variability in the distribution of tropospheric O_3. Map types featuring cyclones near the US east coast (MAM2–MAM5) produced the greatest export to the lower free troposphere with O_3>65 ppbv and O_3-CO slopes ranging 0.25–0.36. HYSPLIT backward trajectories indicated that the high O_3 levels were possibly a result of pollutants lofted to the free troposphere by the warm conveyor belt (WCB) of a cyclone. An important finding was that pollutant export occurred in the main WCB branch to the east of the cyclone and in a secondary branch circling to the back of the cyclone center. Conversely, a map type featuring a large anticyclone dominating the flow over the US east coast (MAM6) restricted export with O_3 levels generally <45 ppbv and an O_3-CO slope near zero. There was also evidence of stratospheric intrusions particularly to the north of 45° N in the 316 hPa composites predominately for MAM1 which featured a large cyclone near Newfoundland. However, it was not clear from the available data that these intrusions had a strong impact on the 681 hPa O_3 composites in the western North Atlantic Ocean further south where the data showed clear evidence of the influence of pollutant export.

ACPD

8, 19743–19789, 2008

1 Introduction

The tropospheric ozone (O_3) column abundance sheds insight on the influence of anthropogenic activities on the global atmospheric composition. For decades the tropospheric O_3 column was estimated based on the satellite measurements of the total column and the stratospheric profile due to lack of tropospheric vertical profiles (Fishman et al., 1990, 2005; Creilson et al., 2003; Stohl et al., 2003a). These estimates were highly uncertain, and it was difficult to obtain an understanding of vertical transport of surface pollutants and stratospheric intrusions.

The launch of EOS-AURA on 15 July 2004 with the Tropospheric Emission Spectrometer (TES) onboard, enabled for the first time, quantification of the tropospheric column and profile of O_3. TES is a Fourier transform infrared spectrometer designed to measure global distributions of tropospheric O_3 and its precursors such as carbon monoxide (CO) (Beer et al., 2001). These measurements may prove to be crucial for the study of many global air quality problems, including the estimation of intercontinental transport (ICT) of pollutants exported from North America.

North American outflow can travel from within the continental boundary layer to the Atlantic Ocean by low-level westerly winds, and portions of these plumes may be incorporated into the marine free troposphere because of the difference in continental and marine boundary layer structure (Angevine et al., 2004; Rodrigues et al., 2004). This scenario enables O_3 to be slowly transported across the Atlantic Ocean (~10 days transport times in summer months) at low levels (2–4 km) but cut-off from the destructive (halogen) chemistry of the MBL (Owen et al., 2006). Pollutants may also be transported from the continental boundary layer in a warm conveyor belt (WCB) of a synoptic-scale cyclone into streams of fast moving middle and upper tropospheric westerly winds (Eckhardt et al., 2004; Crielson et al., 2003; Stohl et al., 2003a). Some WCBs originating over North America can transport O_3 and precursors to the free troposphere over Europe within 4–5 days where descending motions carry them back toward the surface causing ground-level O_3 mixing ratios to rise (Huntreiser et al.,

ACPD
8, 19743–19789, 2008

2005). However, complicating the quantification of contributions from distant sources is that the same cyclones responsible for lofting O_3-forming anthropogenic pollutants from the continental boundary layer to the free troposphere may also mix down O_3 of stratospheric origin (Cooper et al., 2001, 2002; Moody et al., 1996; Merrill et al., 1996; Oltmans et al., 1996; Polvani and Esler, 2007). Thus information on the 3-dimensional distribution of O_3 and its precursors is required to ascertain the contributions of the various sources to observed O_3 levels.

A number of field missions (e.g., NARE, ITCT-2K2, NEAQS2002, and INTEXA/ICARTT2004) have been dedicated to understanding the composition of North American outflow (e.g., Parrish et al., 1993, 1998; Banic et al., 1996; Berkowitz et al., 1996; Cooper et al., 2001, 2002, 2005; Fehsenfeld et al., 2006; Singh et al., 2006; Mao et al., 2006). In many of these studies critical vertical information was obtained via highly coordinated measurement programs involving ozonesonde networks, ships and aircraft, which were only feasible for short intensive study periods over limited areas and are conceivably rather sparse. Therefore long-term continuous measurements over extensive areas had been missing for the vertical structure of the atmospheric composition.

A few modeling studies have complimented the field campaigns by examining 3-dimensional distributions of O_3 over the North Atlantic and Europe as a result of North American outflow for extended periods (Kasibhathatla et al., 1996; Jacob et al., 1993; Li et al., 2005; Auvray and Bey, 2005). However, uncertainties in emissions profiles, the lack of observations for the initialization of chemical fields, and the inherent uncertainties in the modeling of atmospheric circulations and chemical processes present significant challenges in interpretation of the results (Auvray et al., 2007).

The ultimate application of TES measurements is to help address some of these challenges by providing a continuous independent 3-dimensional observational data base for comparison and eventually as a source of model input through data assimilation techniques. However, they must first be thoroughly examined and evaluated for accuracy and information content. Such efforts are currently ongoing and have in-

ACPD
8, 19743–19789, 2008

cluded the statistical validation of TES O_3 profiles against global sets of ozonesondes (Worden et al., 2007; Nassar et al., 2008) and comparisons with aircraft and ground-based measurements over the highly polluted regions such as Mexico City (Shim et al., 2007). Zhang et al. (2006) have examined North American export and found a positive correlation between lower-middle tropospheric TES O_3 and CO downwind of the US for July 2005. However, a yet unexplored critical issue to the study of North American export is how these measurements respond to the highly variable circulation patterns that affect the continental east coast and in particular the northeastern US and adjacent Atlantic Ocean.

Tropospheric O_3 levels in many locations in the Northern Hemisphere show a distinct seasonal variation with levels peaking in spring and remaining high during the summer months (Monks, 2000). However, the frequency of mid-latitude cyclones and anticyclones decreases in summertime and circulation over the eastern US and western North Atlantic tends to be dominated by the large persistent subtropical Bermuda/Azores High (Ziska and Smith, 1980; Key and Chan, 1999; Owen et al., 2006). Therefore, in this study we focused on the spring, i.e., March, April, and May (MAM), and classified the TES retrievals during for this season for 2005 and 2006 by circulation type over a domain covering the eastern US, southeastern Canada and the adjacent western North Atlantic Ocean. We aimed to examine possible associations between the variability in O_3 captured in TES observations and synoptic-scale atmospheric circulations which regulate transport and dispersion of pollutants in the North American export region.

2 Data and methods

2.1 TES Data

Aura is in near polar, sun-synchronous orbit around the Earth with an ascending equatorial crossing at approximately 13:45 local time (Schoeberl et al., 2006) (http:

//aura.gsfc.nasa.gov). Onboard Aura, TES scans the atmosphere in the infrared to measure O_3 and O_3 precursors such as CO. TES produces a 16-orbit Global Survey every other day while the alternate days are reserved for special observations over selected parts of the globe. For this study we used the TES Level 2 V002 Global Survey data (Osterman et al., 2007a) during MAM of 2005 and 2006. The nadir on-the-ground footprint is approximately 5.3 km×8.4 km (Bowman et al., 2002; Beer et al., 2001; Beer et al., 2006). The along-orbit spacing between footprints for the Global Survey runs was approximately 544 km before 25 May 2005 but improved to approximately 182 km after the limb scans were eliminated and replaced by an additional nadir scan (Osterman et al., 2007b). Each orbit was approximately 22° longitude apart. TES vertical coverage extends from 0–~33 km and in cloud-free conditions the vertical resolution is approximately 6 km with sensitivity to both lower and upper troposphere as well as the stratosphere (Bowman et al., 2002; Worden et al., 2004).

Atmospheric parameters are retrieved from the measured TES radiances using algorithms described by Rodgers (2000), Worden et al. (2004) and Bowman et al. (2002, 2006a). The retrieved vertical profiles can be related to the true profiles and a priori constraint profiles with the relationship:

$$\hat{\boldsymbol{x}} = \boldsymbol{x}_c + \mathbf{A}(\boldsymbol{x} - \boldsymbol{x}_c) \quad (1)$$

The vectors $\hat{\boldsymbol{x}}$, $\boldsymbol{x}$ and $\boldsymbol{x}_c$ represent the retrieved, true and a prior constraint profiles. Since the measured TES radiances are affected by a significant vertical extent of the atmosphere, the true state at any given atmospheric level can influence the retrieved state values at many adjacent levels. The averaging kernel matrix **A** defines the contribution of the each element of the true state vector to the retrieval at a particular pressure (or altitude) level. For example, the averaging kernel for a retrieved profile near 31° N and 74° W on 6 April 2006 indicated that the 681 O_3 estimate was affected by the true state O_3 profile not only at 681 hPa but from all levels between approximately 900 and 450 hPa (Fig. 1). This vertical smoothing effect which varies from profile to profile based on the meteorological parameters such as temperature humidity and cloud cover

ACPD
8, 19743–19789, 2008

as well as the vertical distribution of O_3 or CO must be factored into any interpretation of the TES measurements.

A weakness of TES is its general inability to accurately measure boundary layer parameters for typical atmospheric conditions, except in regions where surface temperatures are over 300 K and the temperature contrast between the surface and the air is larger than 10 K (Worden, J., et al., 2007). However, retrievals of the lower free troposphere may show evidence of pollutants recently lofted from the boundary layer. In the context of the vertically smooth averaging kernels of the TES measurements we consider the lower free troposphere to range from approximately 850–550 hPa. For that purpose we chose to examine the O_3 and corresponding CO distributions at the 681 hPa retrieval level for which TES should have good sensitivity. We also examined the distributions at the 316 hPa level to contrast the upper and lower tropospheric distributions and to gain insight into different mechanisms controlling the lower free tropospheric O_3 in the export region of North America.

The TES retrieval products contain diagnostic information and flags for screening out failed profiles or those with reduced sensitivity (Osterman et al., 2007b; Kulawik et al., 2006). We used the general retrieval quality flag which removes the most suspect profiles. In addition, we screened for clouds since they can impact the retrievals. For instance, Kulawik et al. (2006) estimated that the TES sensitivity to O_3 below a cloud with an optical depth of 1.0 will drop to approximately 30% of the clear sky sensitivity. The TES retrievals included information on cloud optical depth and cloud top pressure. We used cloud top pressure thresholds of 700 and 350 hPa respectively for the 681 hPa and 316 hPa measurements respectively. The choice of a cloud optical depth threshold is complicated by the fact that the sensitivity below the cloud is influenced not only by the cloud optical depth, but also the temperature, surface conditions, and O_3 concentration. However, simulations of O_3 retrievals seemed to indicate that errors in retrieved total column and tropospheric column in the presence of low clouds increased at optical depths of 0.75 and above (see Fig. 7, Kulawik et al., 2006). Therefore we screened out any retrieval with an average cloud optical depth in the 1000–1250 cm^{-1}

ACPD
8, 19743–19789, 2008

O_3 retrieval band greater than this value. For consistency we used the same optical depth threshold for the CO retrievals but also included the average cloud optical depth in the 2000–2200 cm^{-1} CO band. We also screened for overall measurement sensitivity at the given retrieval level using the averaging kernel matrix, which is provided as a post-processing diagnostic, by eliminating those profiles for which the diagonal value at the level we were examining (681 or 316 hPa) was less than 0.01.

TES retrievals use the optimal estimation approach described by Rodgers (2000). The retrievals require an a priori constraint to insure mathematical uniqueness. For O_3 and CO the constraint consists of a prior profiles and covariance matrices from a climatology developed using the MOZART model (Brasseur et al., 1998). The climatological a priori is made up of MOZART profiles averaged monthly over 10°×60° latitude-longitude boxes (Bowman et al., 2006). The geographically variable a priori adds artificial structure, which can potentially obscure some of the real geographical variability of a trace gas. This artifact can be removed by reprocessing the TES O_3 and CO profiles with a universal a priori using a procedure developed by Zhang et al. (2006). We generated a universal a priori by averaging all original a prior profiles in the 60° N–60° S band and reprocessed the TES O_3 and CO data following Zhang et al. (2006). Hereafter in this study all of the TES data presented will refer to the reprocessed data.

2.2 Meteorological analyses

We used Global Final Analysis (FNL) data from the National Centers for Environmental Prediction (NCEP) to identify the predominant atmospheric circulation patterns over eastern North America and the North Atlantic Ocean during the time period 2000–2006. FNL products are available for 4 time intervals each day (00:00, 06:00, 12:00, and 18:00 UTC) on a 1°×1° horizontal grid at the surface and 26 pressure levels vertically ranging from 1000 to 10 hPa (http://dss.ucar.edu/datasets/ds083.2).

In addition, we used HYSPLIT (Draxler and Rolph, 2003, http://www.arl.noaa.gov/ready/hysplit4.html) backward trajectories to aid us in determining the likely source

ACPD
8, 19743–19789, 2008

regions for any O_3 and CO enhancements observed in the TES data downstream of North America. The HYSPLIT model was used in single trajectory and ensemble mode with both Global Data Assimilation System (GDAS) (Derber et al., 1991; http://www.arl.noaa.gov/ss/transport/gdas1.html) and Eta Data Assimilation System (EDAS)http://www.arl.noaa.gov/ss/transport/edas40.html inputs. The GDAS data were on a $1^\circ \times 1^\circ$ global grid and with vertical coverage from the surface to 20 hPa. The EDAS data were on a horizontal grid with 40 km spacing centered over the continental US and extending northward into Canada to approximately 60° N, southward into Mexico to approximately 15° N, westward into the Pacific Ocean to approximately 140° W and eastward into the Atlantic Ocean to approximately 60° W http://www.arl.noaa.gov/data/archives/edas40/EDAS40.gif The EDAS data extended vertically from the surface to 50 hPa. In the ensemble mode HYSPLIT generates a set of 27 trajectories by shifting the meteorological input fields by one grid point each in the east, west and vertical directions. By doing so the ensemble gives the probable range of possible trajectories from a given location. This is helpful for circulation patterns with a high degree of spatial variability in which a small error in the selection of the starting point or in the meteorological input fields can result in large differences in trajectory pathways.

We also investigated the link between observed tropospheric O_3 enhancements and stratospheric intrusions using isentropic potential vorticity from the NCAR/NCEP $2.5^\circ \times 2.5^\circ$ Reanalysis (NNRA, http://www.cdc.noaa.gov/cdc/reanalysis. The NNRA isentropic potential vorticity analyses were available 4 times per day (00:00, 06:00, 12:00, and 18:00 UTC) at 11 isentropic levels for 270, 280, 290, 300, 315, 330, 350, 400, 450, 550, and −650 K. We interpolated these data to constant pressure levels to facilitate use with NCEP FNL analyses and TES retrievals which were also on pressure levels.

2.3 Circulation classification

Synoptic-scale circulation patterns over the North Atlantic were classified by applying the correlation-based map typing algorithm of Lund (1963) to the NCEP FNL SLP fields.

This technique has been successfully applied to synoptic classification of summertime circulation patterns over the northeastern United States using the NCEP grids (Hegarty et al., 2007). In brief, the algorithm calculates a correlation coefficient between the grids representing scalar meteorological analysis fields over a given spatial domain at different times. The map types are selected using a critical correlation coefficient (i.e., 0.6), and then all the days in a given study period are classified as one of these types based on the degree of correlation.

Typically either the SLP or upper-level geopotential height (GPH) fields are chosen to represent the circulation patterns in the map typing algorithm. We found that, in comparison to SLP, the classification of the upper-level GPH was much less accurate with many patterns being incorrectly classified based on our subjective judgment of a representative sample. This is because the upper-level GPH fields tended to have smoother and less distinct features than SLP. Therefore we settled on using the SLP fields which are usually correlated with the upper-level patterns and yet exhibit distinctly synoptic features such as fronts, WCB and dry intrusions.

The map typing domain extended from 35° N to 50° N latitude and from 80° W to 50° W longitude (Fig. 2a). It covered much of the northeastern coast of the United States including the Washington D.C. to Boston megalopolis and extended eastward about a third of the way across the North Atlantic Ocean. The dimensions of the map typing domain were chosen to be just large enough to identify the unique synoptic features of each circulation pattern along the mid-latitudes of the North American east coast, which we hypothesized to be important controls on pollutant export, but small enough to insure accuracy of the synoptic classification. Synoptic patterns over larger domains are more difficult to classify because of the additional spatial variability inherently present over a greater area. To examine the larger-scale impact of the circulation patterns on the tropospheric distributions of O_3 and CO exported from North America the map typing domain was embedded into a larger study domain which extended from 25° N to 60° N and from 90° W to 40° W (Fig. 2a).

ACPD
8, 19743–19789, 2008

3 Synoptic circulation classification

We classified days based on six map types (denoted as MAM1–MAM6) identified for the spring seasons of 2005–2006 when TES V002 data was available. The map type frequencies and the important meteorological features associated with each map type are summarized in Table 1. Here we present a brief discussion as to how the patterns might relate to the major hypothesized transport pathways. In Sect. 4 we discuss in detail the impact of these circulation patterns on the tropospheric O_3 distributions observed by TES.

Map type MAM1 was the most frequent pattern, occurring on 24% of the days in springs 2005–2006 (Table 1). It featured a large, intense, and closed low centered east of Newfoundland, Canada (Fig. 2a), which was typically the result of a rapidly deepening cyclone migrating northeastward along the US east coast. Often these systems become so large and vertically deep that they disrupt the normal west to east progression of storm systems and they become quasi-stationary. Analysis of the sequencing of map types indicated that MAM1 persisted for 2–4 days in a row with a maximum duration of up to 10 days, particularly early in the season. The persistent pattern could thus produce a well-mixed troposphere by continuous vertical mixing around the center of the low. Another characteristic of MAM1 was that the surface low was typically associated with a closed upper-level circulation that extended above the 300 hPa pressure level and with 400 hPa potential vorticity (PV) >1.4 potential vorticity units (PVU) on its western side (Fig. 3a). The tropopause is typically defined as falling between 1 (Shapiro, 1987) and 2 PVU (Appenzeller et al., 1996; Lamarque et al., 1996; Parrish et al., 2000). Therefore PV values over the range of 1–2 PVU extending down into the troposphere are typically regions of stratospheric intrusions. This indicates that in MAM1 stratospheric influence reached at least as low as the 400 hPa level over south of Newfoundland, which may explain the higher levels of the 681 hPa O_3 in that area as will be discussed in Sect. 4.1.

Map types MAM2–5 depict smaller and generally more mobile cyclones near the

ACPD
8, 19743–19789, 2008

east coast (Fig. 2b–f). These systems occurred on a total of 50% of the spring days in 2005–2006 and typically featured distinct ascending and descending air streams (Table 1). The WCB, one of the main ascending streams, is located to the east of the cold front and generally originates in the lower troposphere (Carlson, 1980; Eckhardt et al., 2004). It is evident as a sharp trough and rises into the middle and upper troposphere on a general southwest to northeast trajectory (Fig. 2b). The WCB may be intercepted by the fast moving upper level winds that transport pollutants rapidly downstream of the cyclone. This process has been documented through aircraft measurements (Cooper et al., 2001, 2002; Parrish et al., 2000; Stohl and Trickl, 1999; Stohl et al., 2003b; Trickl et al., 2003). Note that a part of the airstream originating in the WCB may branch off to the west and then turn south due to strong easterly and northeasterly cyclonic flow in the lower free troposphere encircling the low center (Fig. 2b). This pathway, described as a secondary WCB, could also be an important mechanism for transporting pollutants from the urban areas of the US east coast to the lower free troposphere of the western North Atlantic. The other major ascending air stream is the cold conveyor belt (CCB) (Fig. 2b) (Carlson, 1980). For east coast cyclones this airstream typically originates from the lower troposphere over the ocean where it intercepts primarily aged air. Furthermore, it occurs characteristically within very cloudy regions not conducive to photochemical production of O_3 (Cooper et al., 2001, 2002).

The main descending airstream of the cyclone is usually referred to as the dry airstream (DA) (Fig. 2b) because it transports drier air from the upper troposphere and in some cases lower stratosphere to the middle and lower troposphere (Carlson, 1980; Cooper et al., 2002). Along with low humidity the air transported in the DA is also normally O_3-rich and therefore influences the O_3 distributions of the lower troposphere (Cooper et al., 2001, 2002; Moody et al., 1996; Merrill et al., 1996; Oltmans et al., 1996).

The differences in the map types MAM2–MAM5 were mainly in the position and history of the cyclones. The cyclones depicted in MAM2 were generally mature systems that had tracked from the central US to the Canadian Maritimes over several days. The

ACPD
8, 19743–19789, 2008

WCB of these systems possibly encountered many high emission regions of eastern North America. The MAM3 map type depicted cyclones that developed along the US east coast with areas of easterly flow in northeastern states. In late spring the MAM3 pattern tended toward episodes of persistence as small cyclones developed along the coast to the east of an inland upper-level cut-off low, and then stalled along the coast or rotated back around the inland system. For example in both May 2005 and 2006 there were episodes of MAM3 which persisted for 6 days or more. The cyclones in MAM4 and MAM5 were offset from the US coast by anticyclones which possibly enabled the DA to influence areas of the western North Atlantic Ocean as will be discussed in Sect. 4.

The final map type, MAM6, occurred on only 7% of the days during springs 2005 and 2006. It featured a subtropical anticyclone centered off the east coast extending well out to sea and westward into the southeastern US. Such a system would typically produce a large area of subsidence extending from the east coast to the central North Atlantic Ocean. This subsidence would likely restrict synoptic-scale lofting of boundary layer pollutants to the free troposphere. This pattern also featured a small cyclone well to the northeast of Labrador. At this northerly location the cyclone possibly had less influence on regulating direct pollutant transport from the populated urban areas of the eastern US and southeastern Canada than the anticyclone to the south.

4 Association between O_3 distributions and circulation types

Composites of the 681 hPa and 316 hPa O_3 and CO for the entire season and individual map types were created by interpolating measurements from the orbital overpasses to a $1^\circ \times 1^\circ$ grid using a Gaussian weighting scheme similar to that described in Luo et al. (2002). If no observations existed within 350 km of a grid point, typically because of quality or cloud screening, this point was masked out of the analysis.

First, we created full seasonal composites for the 681 hPa O_3 and CO which included all the observations regardless of map type (Fig. 4). The mean 681 hPa O_3

ACPD
8, 19743–19789, 2008

seasonal composite indicated elevated levels (55–65 ppbv) over the western Atlantic Ocean south of 45° N, ~1000 km downwind of the US (Fig. 4a). There was a corresponding feature in the mean CO composite with mixing ratios of 115–125 ppbv forming a belt emanating from the US east coast that dissipated and narrowed before turning northeastward following the prevailing lower tropospheric wind flow (Fig. 4b). In the area of highest CO extending from the US coast, between 75° W–55° W and 30° N–45° N (denoted hereafter as Region 1), we found a positive correlation of 0.32 between O_3 and CO with a slope of 0.16 (Fig. 5a and Table 2). However, further to the north and east in a region bounded by 45° N–55° N and 65° W–45° W (referred to hereafter as Region 2), where O_3 gradually dropped off to 50–55 ppbv, there was no O_3-CO correlation (Fig. 5b, Table 2).

The correlation of observed O_3 and CO is a useful diagnostic indicator of the photochemical processing of an air mass, and the O_3-CO slope value can be used to estimate the influence of exported anthropogenic pollutants and the efficiency of photochemical O_3 production (Parrish et al., 1993, 1998; Mao et al., 2004). A large number of measurements at surface sites in eastern North America have indicated that typical summertime O_3-CO slopes range from 0.2–0.35 (Parish et al., 1993, 1998; Chin et al., 1994; Mao et al., 2004). Aircraft measurements during the NARE93 and ICARTT 2004 summer campaigns indicated similar slopes, which took place in the lower free troposphere just east of the North American coastline (Daum et al., 1996; Zhang et al., 2006).

Fewer studies have been conducted for springtime, but analysis of spring measurements over 4 years in the 1990s at Sable Island, Nova Scotia indicated that the O_3-CO slope increases dramatically from near zero in March to approximately 0.35 in May (Parrish et al., 1998). Our free tropospheric value of 0.16 in the Region 1 falls in the middle of this range and suggests that similar to summertime the pollutant plumes lofted to the free troposphere retain their near surface features. In Region 2, the lack of O_3-CO correlation indicated no significant photochemical production due to either limited sunshine or the lack of fresh exported pollutants. The fact that this area showed

a relative minimum in CO (Fig. 4b) suggests that the lack of exported pollutants was a more critical factor.

All the TES retrievals for the months of March–May 2005 and 2006 were also grouped based on the map type classification for the calendar day of the orbital overpass. The O_3 and CO distributions corresponding to the 6 map types are now discussed.

4.1 MAM1

The 681 hPa O_3 levels for MAM1 were slightly elevated (~55–60 ppbv) in a region extending from the Canadian Maritimes southward over the western North Atlantic Ocean (Fig. 6a). The circulation pattern, featuring the intense persistent low near Newfoundland, produced distinct chemical characteristics in Regions 1 and 2 reflected in the O_3-CO relationship (Figs. 6a, g, 7a and b). Region 2 featured O_3 mixing ratios >60 ppbv and relatively low CO (<100 ppbv) (Fig. 7g) yielding a negative O_3-CO correlation of $r=-0.14$ (Fig. 7b, Table 2). This region was also associated with an extensive area of elevated O_3 (>160 ppbv) at the 316 hPa level (Fig. 8a) and elevated PV values (>1.5 PVU) at the 400 hPa level (Fig. 3a). All of these factors indicated that the elevated tropospheric O_3 mixing ratios in Region 2 over the Canadian Maritimes were likely a result of stratospheric inputs associated with the deep low pressure system. It should be cautioned that this enhancement in 681 hPa O_3 could also be technically a result of a shift toward higher altitudes (400–500 hPa) of the peak 681 hPa O_3 averaging kernels (not shown) in retrieval calculations. Regardless, the elevated tropospheric O_3 was likely not a direct result of pollutants recently exported from North America.

Region 1 had a large offshore area of 681 hPa composite O_3 mixing ratios ranging from 55 to 60 ppbv corresponding to a belt of slightly elevated CO (120–125 ppbv) (Fig. 6a and g). The presence of both elevated O_3 and CO levels in Region 1 produced a positive O_3-CO correlation of 0.32 (Fig. 7a, Table 2) indicating anthropogenic influence. Anthropogenic pollutants were most likely injected into the large circulation system by the mobile cyclone preceding the development of the large semi-stationary

ACPD
8, 19743–19789, 2008

cyclone or other smaller cyclonic systems that may have traveled southeastward along the southwest corner of the main circulation. HYSPLIT trajectories generated using GDAS meteorological data for a MAM1 case persisting from 15–21 March 2006 indicted that air at levels near 681 hPa could completely circulate around the cyclonic system within 3 days. Thus suggesting that pollutants entrained into these types of circulation patterns could potentially circulate around several times, at least for the longest duration cases, and be gradually diluted or chemically decomposed resulting in a uniform moderate enhancement in CO levels.

4.2 MAM2 and MAM3

The smaller, more dynamic cyclonic systems located near the US coast in MAM2 and MAM3 produced O_3 and CO composite distributions with greater contrast between areas of high and low mixing ratios compared to those in MAM1. At 681 hPa there was a general area of elevated O_3 mixing ratios (>60 ppbv) extending from just off the US coast to ~50° W south of ~45° N (Fig. 6b and c). Elevated O_3 roughly corresponded to increased CO (>120 ppbv), particularly near the US coast (Fig. 6h and i). The location of the elevated O_3 and CO to the east of storm centers and downwind of the US coast suggests that lofting of the pollutants from the continental boundary layer by the WCB airstreams played a major role in producing the observed O_3 levels for these map types.

There were some differences in the 681 hPa O_3 and CO distributions between MAM2 and MAM3. For example the area of high O_3over the ocean for MAM2 was generally off of the US coast at latitudes north of the Carolina states, whereas for MAM3 it extended all the way to the coast and even inland. In addition, the CO enhancement in MAM3 was less and dropped off to the east more quickly than in MAM2. These differences are possibly due in part to the circulation patterns. The MAM2 circulation features a predominant low over land with basically west to southwest flow at the coast, while the high and low pair in MAM3 resulted in an easterly component to the flow along the northern parts of the coast. Thus, for MAM2 the pollutants would be transported away from the coast, while for MAM3 some of the continental outflow might be re-circulated

ACPD
8, 19743–19789, 2008

back toward the coast.

In general, we found that the 681 hPa O_3 and CO observations for map types MAM2, and MAM3 were positively correlated at r=0.44 and 0.42, respectively, in Region 1 with corresponding slopes of 0.24 and 0.25 (Fig. 9, Table 2). These slopes are about one third as large as those reported by Zhang et al. (2006), who calculated a slope of 0.81 and a correlation of r=0.53 for lower tropospheric TES measurements near this region. However, this may be partially explained by the fact that their measurements were in July for a more compact region centered further south, while ours included a larger region centered further north and included the months of March and April when photochemical production is reduced.

The DAs of the cyclones in MAM2 and MAM3 may have potentially transported stratospheric air down to tropospheric levels. At 316 hPa the O_3 distributions for MAM2 and MAM3 were generally anti-correlated with the lower levels as most of the highest mixing ratios were poleward of 50° N (Fig. 8b and c). The exceptions were areas of elevated O_3 near the mean position of the upper level trough associated with the surface cyclones and were likely due to lower tropopause levels and stratospheric intrusions as suggested by somewhat higher PV values (Fig. 3b and c). The fact that the 316 hPa and 681 hPa distributions show little spatial correlation suggests different processes dominating at the two levels. For instance, contributions from continental boundary layer pollution may have played a significant role in the occurrence of elevated O_3 over western North Atlantic, especially south of 45° N on the 681 hPa level.

Since WCB lofting to the upper troposphere is an important mechanism for continental export of pollution, we examined the TES 316 hPa composites for evidence of this transport mechanism. The CO composites showed areas of elevated CO off the southeastern US coast particularly for MAM2 and MAM3. Correspondingly there were areas of elevated CO in the lower troposphere (Fig. 6g and h). It is possible that the pollutants were lofted to the upper troposphere by convection possibly associated with the cold fronts of the passing cyclones as suggested in previous studies (Kiley and Fuelberg et al., 2003; Li et al., 2006 and Kim et al., 2008). However, this speculation was not

ACPD
8, 19743–19789, 2008

supported by upper tropospheric backward trajectories from this region for the 3 days featuring the highest 316 hPa TES retrievals (CO>115 ppbv), since these trajectories, calculated using EDAS meteorological data, did not intersect the lower troposphere over the US This is possibly because convective processes are sub-grid scale features (>40 km grid spacing of EDAS) and were not resolved in the trajectory analysis.

The 316 hPa composite CO for MAM2 did reveal that the region just southeast of Newfoundland with CO >150 ppbv was likely influenced by continental export. Upper tropospheric backward EDAS trajectories, for 2 of the 3 days coincident with the highest CO mixing ratios in this region indicated the source was boundary layer air over the US Central Plains that was mixed with air that had traveled near the surface from the western Gulf of Mexico and near the Los Angeles Basin (not shown). These results suggested that the significant upper level CO features of our composites mainly resulted from transport from distant sources. It is possible that east coast emissions rise slowly while moving rapidly in a general northeastward direction in the WCB and thus would not yet have ascended to this level within the confines of our study domain.

4.3 MAM4 and MAM5

The meteorological conditions of map types MAM4 and MAM5 differed from MAM2 and MAM3 in that the cyclones were displaced from the coast by anticyclones resulting in significant contributions from both the WCB and DA airstreams. For both MAM4 and MAM5 there were elevated O_3 levels (>55 ppbv) over the western North Atlantic Ocean extending from the coast of Florida northeastward to east of Newfoundland (Fig. 6d and e). Some areas, e.g., off the coast of the southeastern US with both elevated O_3 and CO, were likely produced by WCB lofting of continental pollutants (Fig. 6j and k). However, there were other areas of elevated O_3 that corresponded to relatively low CO (<110 ppbv). For example, for MAM5 high O_3 was coupled with low CO near 40° N and 60° W which seemed to be due to stratospheric inputs. This was evidenced by elevated O_3 and PV at 316 hPa and 400 hPa PV in both composites (Figs. 3e and 8e). In addition, based on the position of the surface cyclone this would have been

ACPD
8, 19743–19789, 2008

the location of the DA which characteristically facilitates downward transport from the upper troposphere. It should be noted that as with MAM1 there was a corresponding shift toward higher altitudes of the 681 hPa O_3 averaging kernels with the stratospheric intrusion region. However, for MAM5 the averaging kernel peaks shifted upward to only 500–550 hPa and thus it seems more likely that for MAM5 the high levels of 681 hPa O_3 retrieved by TES in this region were actually due to high O_3 levels in the lower free troposphere.

It was more difficult to identify for MAM4 the mechanisms controlling areas of high O_3 coupled with low CO. An area of high 681 hPa O_3 and relatively low CO extended from east of Newfoundland southwestward to just east of Bermuda (Fig. 6d and j). The 316 hPa O_3 composite showed a lobe of high O_3 extending southwestward from the central north Atlantic near to Florida, whereas the 400 hPa PV composite did not show this feature (Figs. 8d and 3d). This apparent contradiction could possibly be explained by the combination of poor TES data coverage for this map type and the occurrence of a single strong stratospheric intrusion. Because of the low frequency of MAM4 in 2005 and 2006 (7% of the days, Table 1) and occasional missing Global Surveys this type had the fewest days (only 5) contributing to the composites. This allowed individual episodes to be overrepresented in the composite analysis in some areas. One case significantly influencing the composite analysis occurred on 25 May 2006 when an unusually strong stratospheric intrusion extended down to Bermuda from a cyclone to the northeast. This event produced several retrieved profiles with 681 hPa O_3 mixing ratios >90 ppbv and CO over 95–100 ppbv in a region just north and east of Bermuda. In general, the distributions over the western North Atlantic Ocean south of 40° N were controlled by outflow from the inland cyclone, as evidenced by the slope of O_3-CO slope of 0.36 in Region 1 (Table 2). The case of 25 May 2006 demonstrated the possible influence of stratospheric intrusions in this region. However, scarce data coverage made it impossible to determine whether these occurrences were a dominant mechanism in this region for this map type.

ACPD
8, 19743–19789, 2008

4.4 MAM6

The lowest 681 hPa O_3 levels in the western Atlantic corresponded to circulation patterns of MAM6. For this map type composite O_3 levels in the western Atlantic were generally below 55 ppbv with many areas, especially close to the US east coast, being below 45 ppbv (Fig. 6f). The 681 hPa CO mixing ratios were also low in the western Atlantic with composite values generally below 110 ppbv (Fig. 6l). There was nearly no correlation between O_3 and CO in Region 1 (Table 2), which implied that air masses in this region were photochemically aged and intermixed. We hypothesize that the large surface anticyclone centered near Bermuda and extending westward into the eastern US and eastward well out to sea may have produced large-scale subsidence conditions which were unfavorable for lofting pollutants into the lower free troposphere. The only area of high 681 hPa O_3 in the western North Atlantic Ocean was near Newfoundland and was likely associated with stratospheric intrusions. This area corresponded to the location an area of elevated 400 hPa PV (Fig. 3f) and a region of elevated O_3 at 316 hPa with O_3 levels exceeding 160 ppbv (Fig. 8f).

The composite figures of O_3 and CO include instantaneous measurements from different times and locations, whereas the map types reflect the average state of circulation patterns. Naturally it is difficult to make a direct link between the two when the temporal and spatial scales of a pollution event and a weather system are not directly comparable. There are indeed many details in O_3 and CO distributions that need to be interpreted using instantaneous measurements. We thus examined many individual cases to determine the likely export pathways and we present two key illustrative examples in the next section.

5 Export case studies

Two examples are discussed in this section to illustrate how pollutants are transported from the continent to the lower free troposphere over the western Atlantic Ocean by

ACPD
8, 19743–19789, 2008

cyclones under specific map type conditions. Both involve transport via the WCB but depict different locations for the O_3 enhancements with respect to the position of the cyclone.

The first example was a case of MAM2 on 2 April 2006 when high O_3 and CO at 681 hPa was measured by TES in the main branch of WCB airstream. On 31 March a compact surface low pressure system was located over the upper Midwest and a surface high pressure was located just off the South Carolina coast producing general southwesterly flow from the eastern Gulf of Mexico toward the northeastern states. The low pressure center tracked eastward and elongated in the north-south direction during the next two days while the high moved further off shore. By 12:00 UTC the surface low center was located over New Brunswick Canada with a sharp trough extending southward just off the east coast (Fig. 10a).

The TES retrieved 681 hPa O_3 exceeding 70 ppbv and 681 hPa CO exceeding 140 ppbv near the intersection of 40° N and 60° W during the afternoon ascending overpass (Fig. 10b). From the cloud pattern the high pollutant levels appeared to be in the WCB branch of the cyclonic system. On the northwestern side of the cloud band marking the WCB the O_3 level decreased to 45–50 ppbv and CO to ~120 ppbv. An ensemble of backward trajectories using EDAS meteorological data (Fig. 10c) from near the locations of elevated O_3 and CO retrievals confirmed that these parcels were part of a slowly ascending airstream passing over the southeastern US boundary layer and eastern Gulf of Mexico during the previous 2–3 days where they potentially entrained anthropogenic pollutants.

The WCB is often an area of thick cloudiness obscuring satellite measurements of lower tropospheric O_3 and CO. For example, in Fig. 10b the orbit is clearly interrupted by the cloud band and resumes on the other side. However, this case demonstrated the ability of TES to measure at least some of the impact of WCB outflow on western Atlantic O_3 levels.

In the second example high O_3 and CO at 681 hPa occurred in mainly clear skies behind the main WCB region on 7 April 2006, a day also classified as MAM2 (Fig. 11).

ACPD
8, 19743–19789, 2008

A low pressure center tracking into southern Canada from the Midwest on 3 April spawned a secondary the New York and New Jersey coast on 4 April (Fig. 11a and b). This new low center became the primary low as it tracked northeastward into the Canadian Maritimes on 7 April (Fig. 11c).

At approximately 06:00 UTC 7 April TES measured high 681 hPa O_3 (>70 ppbv) and CO (120–185 ppbv) on the descending Aura overpass which occurred just south of 40° N and near 63° W (Fig. 11d). An ensemble of HYSPLIT backward trajectories using EDAS meteorological data showed that air parcels passed over the urban areas of the northeastern US in the lower troposphere before ascending into the middle troposphere. In the meantime these air parcels moved northeastward into southeastern Canada then turned cyclonically to the west and eventually southeastward toward the ocean while descending back to the lower troposphere (Fig. 11e). Some of the ensemble members remained in the boundary layer over the east coast urban areas before being lofted into the middle troposphere by the developing storm system on 4 April. These backward trajectories and coincident high CO and O_3 together suggested that the high mixing ratios behind or to the west of the storm center and main WCB were influenced by export of pollutants from the urban northeast corridor of the US.

This is an important finding because high O_3 levels in the lower troposphere to the west of the surface low center have been frequently linked to O_3-rich air descending from the upper troposphere or stratosphere in the DA (Cooper et al., 2001, 2002; Moody et al, 1996; Merrill et al., 1996; Oltmans et al., 1996). The trajectories followed the same general track as the secondary WCB branch designated as W2 by Cooper et al. (2001), in which high O_3 levels were attributed to stratospheric air mixed into the polluted air of the WCB. However, since most of the back trajectories remained in the lower or middle free troposphere and CO levels were high it is possible that a significant amount of the O_3 enhancement was due to anthropogenic contributions. Thus, this case suggests that the W2 branch may also be an important pollutant export stream capable of influencing the O_3 levels over the western North Atlantic Ocean.

ACPD
8, 19743–19789, 2008

6 Evolution of continental outflow

Once out over the ocean the polluted continental air in the free troposphere appeared to have been diluted as the mixing ratios of CO decreased. For instance, the seasonal mean CO mixing ratios at 681 hPa noticeably dropped off to below 120 ppbv east of 55° W (Fig. 4b). However, the 681 hPa O_3 levels remained at almost the same levels across the Atlantic Ocean (Fig. 4a). As a result the seasonal mean O_3-CO slope increased to 0.21 in Region 3 from a value of 0.16 in Region 1 (Table 2). This increase in slope in Region 3 was also evident for 4 out of the 6 map types including the major cyclonic export types of MAM2 and MAM3 (Table 2). One possible explanation for the slower loss rate of O_3 compared to CO, which led to increased O_3-CO slopes, is that O_3 continued to be produced in the plume during transport (Mao et al., 2006). For example, summertime observations at a mountain top site in the Azores have indicated O_3-CO slopes near 1.0 (Honrath et al., 2004), which was attributed to air masses in North American outflow events having undergone days of photochemical processing, producing the high O_3-CO slopes. Another possible explanation for the slower loss rate of O_3 level is that contributions from the upper-level air transported downward in the descending DA air streams of cyclones further east may have also enhanced the lower tropospheric O_3.

One case of high O_3 in the lower troposphere over the central North Atlantic captured by TES measurements occurred on 14—15 May 2006. During the ascending orbit of the afternoon of May 14 and the descending orbit of the following morning TES retrieved a patch of 681 hPa O_3 mixing ratios exceeding 70 ppbv accompanied by only moderate CO levels of 100–115 ppbv between 30°–40° N latitude and 40°–55° W longitude (Fig. 12a and b). The circulation for this period was characterized by a MAM3 map type which persisted during the period of 9–15 May as a large low deepened and stalled over the central US spawning several smaller weaker lows that moved up the east coast. Over the eastern North Atlantic Ocean a large low pressure system persisted near 50° N and 30° W separated from the east coast cyclones by a

ACPD
8, 19743–19789, 2008

high pressure ridge centered over the Canadian Maritimes (Fig. 13a and b). HYSPLIT ensemble backward trajectories using GDAS meteorological data indicated that any air parcels originating in the North American boundary layer would have taken a long detour into the Arctic middle and upper troposphere before being entrained into the DA of the eastern Atlantic cyclone and transported to the lower troposphere of the central Atlantic (Fig. 13c and d). Furthermore, some of the ensemble members suggested a re-circulation of Atlantic Ocean air. Thus, while exported pollutants from North America undoubtedly contributed to the high O_3 levels, evidence of the emissions would have been significantly diluted by mixing with upper tropospheric air and aged Atlantic air.

A final feature of note regarding evolution of continental outflow was the patches of very high CO and O_3 at the eastern edge of our study domain for MAM6. In this general region composite values of O_3 exceeded 60 ppbv and CO exceeded 140 ppbv (Fig. 6f and l). Backward trajectories using GDAS meteorological data (not shown) from retrieval locations of both high CO and O_3 exhibited a wide variety of paths indicating source regions including North America, but also regions to the south and east. The large uncertainty of this analysis was possibly due to the fact that this region was so far east that the circulation pattern depicted by MAM6 had less influence on the O_3 and CO distributions than more local meteorological features. Moreover, the occurrence of the extremely high levels associated with this map type was either coincidental or possibly an indirect result of the relatively weak circulation dynamics of this map type.

7 Summary

The springtime tropospheric O_3 and CO distributions constructed using the 2005 and 2006 TES measurements were dependent on the atmospheric circulation depicted in 6 predominant map types (MAM1–MAM6). The highest O_3 and CO levels in the lower free troposphere of the western North Atlantic Ocean were associated with map types MAM2–MAM5 featuring cyclones near the east coast of the US We hypothesize that these elevated levels were due to lofting of anthropogenic pollutants from the continen-

ACPD
8, 19743–19789, 2008

tal boundary layer via the WCB of cyclones. Case studies for the cyclonic map type MAM2 demonstrated using back trajectories that retrievals of elevated 681 hPa O_3 and CO could be attributed to air parcels encountering the polluted continental boundary layer before being brought to the lower free troposphere by the WCB.

An important finding emerged from this study that boundary layer pollutants were exported to the lower free troposphere via a secondary branch circling around to the back of the cyclone center, in addition to the widely studied transport route facilitated by the main branch to the east of the cold front. This result suggested an additional mechanism for O_3 enhancement in the region which had been considered to be influenced mainly by stratospheric intrusions facilitated by the DA airstream. Also, since this region is typically clearer than the main WCB branch where clouds may obscure many of the TES measurements it is potentially an important region for studying North American export from satellites.

The TES O_3 composites also revealed evidence of stratospheric intrusions associated with the cyclones depicted in the map types. Overall, these features were most pronounced north of 45° N in the western North Atlantic Ocean. However, a complicating issue was that in these regions the averaging kernel tended to shift to higher altitudes and thus observed increases in the 681 hPa O_3 levels were partly due to the fact that the TES retrieval was weighted more toward the upper troposphere.

Composites of TES O_3 and CO retrievals showed the main export band extending from 30° N to 45° N with a seasonal O_3-CO slope of 0.16 at 681 hPa ranging over 0.25–0.36 for the most favorable circulation patterns. The O_3-CO slopes derived from the TES at 681 hPa were consistent with those derived from in situ measurements at ground sites and from aircraft in the lower free troposphere downwind of urban and industrial areas of North America (Parrish et al., 1993, 1998; Daum et al., 1996; Zhang et al., 2006). Once over the ocean the pollutants became diluted as evidence of the drop off in CO levels to the east of 55° W. However, O_3 levels continued to be elevated as a result of continuing photochemical production and in some cases transport of O_3 down from the upper troposphere in the DAs of cyclones further east.

ACPD
8, 19743–19789, 2008

There are problems associated with using satellite retrievals to examine in detail the highly variable tropospheric O_3 distributions, namely the obscuring effects of clouds, the low vertical resolution (i.e. broad averaging kernel peaks), and lack of boundary layer sensitivity. However, the TES retrievals captured a high degree of variability with circulation patterns that was consistent with previous studies of North American export. Therefore, TES measurements incorporated into detailed observational and modeling systems should enable improvements to be made in the study of continental export.

Acknowledgements. The TES Level 2 data were obtained from the NASA Langley Research Center Atmospheric Sciences Data Center. Funding for this work was provided through the NASA Earth and Space Science Fellowship Program under grant NNG05GQ30H.

References

Angevine, W. M., Senff, C., J., White, A. B., et al.: Coastal boundary layer influence on pollutant transport in New England, J. Appl. Meteorol., 43, 1425–1437, 2004.

Appenzeller, C., Davies, H. C., and W. A. Norton: Fragmentation of stratospheric intrusions, J. Geophys. Res., 101, 1435–1456, 1996.

Auvray, M. and Bey, I.: Long-range transport to Europe: Seasonal variations and implications for the European ozone budget, J. Geophys. Res., 110, D11303, doi:10.1029/2004JD005503, 2005.

Auvray, M., Bey, I., Llull, E., Schultz, M. G., and Rast, S.: A model investigation of tropospheric ozone chemical tendencies in long-range transported pollution plumes, J. Geophys. Res., 112, D05304, doi:10.1029/2006JD007137, 2007.

Banic, C. M., Leaitch, W. R., Isaac, G. A., Couture, M. D., Kleinman, L. I., Springston, S. R., and MacPherson, J. I.: Transport of ozone and sulfur to the North Atlantic atmosphere during the North Atlantic Regional Experiment, J. Geophys. Res., 101, 29 091–29 104, 1996.

Beer, R.: TES on the Aura Mission: Scientific objectives, measurements an analysis overview, IEEE Trans. Geosci. Remote Sens., 44(5), 1102–1105, 2006.

Beer, R., Glavich, T. A., and Rider, D. M.: Tropospheric Emission Spectrometer for the Earth Observing System's Aura satellite, Appl. Opt., 40, 2356–2367, 2001.
Berkowitz, C. M., Daum, P. H., Spicer, C. W., and K. M. Busness: Synoptic patterns associated with the flux of excess ozone to the western North Atlantic, J. Geophys. Res., 101, 28 923–28 933, 1996.
Bowman, K. W., Rodgers, C. D. Kulawik, S. S., et al.: Tropospheric Emission Spectrometer Retrieval method and error analysis, IEEE Trans. Geosci. Remote Sens., 44(5), 1297–1307, 2006.
Bowman K. W., Worden, J., Steck, T.,Worden, H. M., Clough, S., and Rodgers, C. D.: Capturing time and vertical variability of tropospheric ozone: A study using TES nadir retrievals, J. Geophys. Res., 107, NO. D23, 4723, doi:10.1029/2002JD002150, 2002.
Brasseur, G. P., Hauglustaine, D. A., Walters, S., et al.,: MOZART: A global chemical transport model for ozone and related chemical tracers: 1. Model description, J. Geophys. Res., 103, 28 265–28 289, 1998.
Carlson, T. N.: Midlatitude Weather Systems, Am. Meteorol. Soc., Boston, 507 pp., 1998.
Chin, M., Jacob, D. J., Munger, J. W., Parrish, D. D., and Doddridge, B. G.: Relationship of ozone and carbon monoxide over North America, J. Geophys. Res., 99, 14 565–14 573, 1994.
Cooper, O. R., Moody, J. L., Parrish, D. D., et al.: Trace gas signatures of the airstreams within North Atlantic cyclones: Case studies from the North Atlantic Regional Experiment (NARE '97) aircraft intensive, J. Geophys. Res., 106, 5437–5456, 2001.
Cooper, O. R., Moody, J. L., Parrish, D. D., et al.: Trace gas composition of midlatitude cyclones over the western North Atlantic Ocean: A conceptual model, J. Geophys. Res., 107, NO. D7, 4056, doi:10l1029/2001JD000902, 2002.
Cooper, O. R., Stohl, A., Eckhardt, S., et al.: A springtime comparison of tropospheric ozone and transport pathways on the east and west coasts of the United States, J. Geophys. Res., 110, D05S90, doi:10.1029/2004JD005183, 2005.
Creilson, J. K., Fishman, J., and Wozniak, A. E.: Intercontinental transport of tropospheric ozone: a study of its seasonal variability across the North Atlantic utilizing tropospheric ozone residuals and its relationship to the North Atlantic Oscillation, Atmos. Chem. Phys., 3, 2053–2066, 2003, http://www.atmos-chem-phys.net/3/2053/2003/.
Daum, P. H., Kleinman, L.I., Newman, L., et al.: Chmeical and physical properties of plumes

ACPD
8, 19743–19789, 2008

of anthropogenic pollutants transported over the North Atlantic during the North Atlantic Regional Experiment, J. Geophys. Res., 101, 29 029–29 042, 1996.
Derber, J. C., Parrish, D. F., and Lord, S. J.: The new global operational analysis system at the National Meteorological Center, Weather Forecast., 6, 538–547, 1991.
Draxler, R. R. and Rolph, G. D.: HYSPLIT (HYbrid Single-Particle Lagrangian Integrated Trajectory) Model access via NOAA ARL READY, NOAA Air Resources Laboratory, Silver Spring, MD, 2003, http://www.arl.noaa.gov/ready/hysplit4.html.
Eckhardt, S., Stohl, A., James, P., Forster, C., and Spichtinger N.: A 15-year climatology of warm conveyor belts, J. Climate, 17, 218–236, 2004.
Fehsenfeld, F. C., Ancellet, G., Bates, T. S., Goldstein, A. H., Hardesty, R. M., Honrath, R., et al.: International Consortium for Atmospheric Research on Transport and Transformation (ICARTT): North America to Europe – Overview of the 2004 summer field study, J. Geophys. Res., 111, D23S01, doi:10.1029/2006JD007829, 2004.
Fishman, J., Watson, C. E., Larsen, J. C., and Logan, J. A.: Distribution of tropospheric ozone determined from satellite data, J. Geophys. Res., 95, 3599–3617 1990.
Fishman, J., Creilson, J. K., Wozniak, A. E., and Crutzen, P. J.: Interannual variability of stratospheric and tropospheric ozone determined from satellite measurements, J. Geophys. Res., 110, D20306, doi:10.1029/2005JD005868, 2005.
Hegarty J. D., Mao, H., and Talbot, R.: Synoptic controls on summertime surface ozone in the northeastern US, J. Geophys. Res., 112, D14306, doi:10.1029/2006JD008170, 2007.
Honrath, R. E., Owen, R. C., Val Martin, M., et al.: Regional and hemispheric impacts of anthropogenic and biomass burning emissions on summertime CO and O3 in the North Atlantic lower free troposphere, J. Geophys. Res., 109, D24310, doi:10.1029/2004JD005147, 2004.
Huntrieser, H., Heland, J., Schlager, C., et al.: Intercontinental air pollution transport from North America to Europe: Experimental evidence from airborne measurements and surface observations, J. Geophys. Res., 110, D01305, doi:10.1029/2004JD005045, 2005.
Jacob D. J., . Logan, J. A, Gardner,J. A., G. M., Yevich, R. M., Spivakovsky, C. M., and Wofsy, S. C.: Factors regulating ozone over the United States and its export to the global atmosphere, J. Geophys. Res., 98, 14 817–14 826, 1993.
Kasibhatla, P., Levy II, H., Klonecki, A., and Chameidas, W. L.: Three-dimensional view of large-scale tropospheric distribution over the North Atlantic Ocean During Summer, J. Geophys. Res., 101, 29 305–29 316, 1996.
Key, J. R. and Chan, A. C. K.: Multidecadal global and regional trends in 1000 mb and 500 mb

cyclone frequencies, Geophys. Res. Lett., 26, 2053–2056, 1999.
Kiley, C. M. and Fuelberg, H .E.: An examination of summertime cyclone transport during Intercontinental Chemical Transport Experiment (INTEX-A), J. Geophys. Res., 111, D24S06, doi:10.1029/2006JD007115, 2006.
Kim, S. Y., Talbot, R., Mao, H., Blake, D., Vay, S., and Fuelberg, H.: Continental outflow from the US to the upper troposphere over the North Atlantic during the NASA INTEX-NA Airborne Campaign, Atmos. Chem. Phys., 8, 1989–2005, 2008, http://www.atmos-chem-phys.net/8/1989/2008/.
Kulawik, S. S., Worden, J., Eldering, A., et al.: Implementation of cloud retrievals for Tropospheric Emission Spectrometer (TES) atmospheric retrievals: 1. Description and characterization of errors on trace gas retrievals, J. Geophys. Res., 111, D24204, doi:10.1029/2005JD006733, 2006.
Lamaraque, J. F., Langford, A. O., and Proffitt, M. H.: Cross-tropopause mixing of ozone through gravity wave breaking: Observation and modeling, J. Geophys. Res., 101, 22 969–22 976, 1996.
Li, Q., Jacob, D. J., Rokjin, P., et al.: North American pollution outflow and the trapping of convectively lifted pollution by upper-level anticyclone, J. Geophys. Res., 110, D10301, doi:10.1029/2004JD005039, 2005.
Luo, M., Beer, R., Jacob, D. J., et al.: Simulated observation of tropospheric ozone and CO with Tropospheric Emission Spectrometer (TES) satellite instrument, J. Geophys. Res., 107(D15), NO.D15, doi:10.1029/2001JD000804, 2002.
Lund, I. A.: Map-pattern classification by statistical methods, J. Appl. Meterorol., 2, 56–65, 1963.
Mao, H. and Talbot, R.: O_3 and CO in New England: Temporal variations and relationships, J. Geophys., Res., 109, D21304, doi:10.1029/2004JD004913, 2004.
Mao, H., R. Talbot, R., Troop, D., Johnson, R., Businger, S., and Thompson, A. M.: Smart balloon observations over the North Atlantic: O3 data analysis and modeling, J. Geophys. Res., 111, D23S56, doi:10.1029/2005JD006507, 2006.
Merrill, J. T., Moody, J. L., Oltmans, S. J., and Levy II, H.: Meteorological analysis of tropospheric ozone profiles at Bermuda, J. Geophys. Res., 101, 29 201–29 211, 1996.
Moody, J. L., Davenport, J. C., Merrill, J. T., et al.: Meteorological mechanisms for transporting O_3 over the western North Atlantic Ocean: A case study for August 24–29, 1993, J. Geophys. Res., 101, 29 213–29 277, 1996.

Monks, P. S.: A review of the observations and origins of the spring ozone maximum, Atmos. Env., 34, 3545–3561, 2000.
Nassar, R., Logan, J. A., Worden, H. M., et al.: Validation of Tropospheric Emission Spectrometer (TES) nadir ozone profiles using ozonesonde measurements, J. Geophys. Res., 113, D15S17, doi:10.1029/2007JD008819, 2008.
Oltmans, S. J., Levy II, H., Harris, J. M., et al.: Summer and spring ozone profiles over the North Atlantic from ozonesonde measurements, J. Geophys. Res., 101, 29 179–29 200, 1996.
Osterman, G., Bowman, K., Cady-Pereira, K., et al.: Tropospheric Emission Spectrometer (TES), validation report, JPL D#102, version 2.0, http://eosweb.larc.nasa.gov/PRODOCS/tes/validation/TESValidationReport_v2_0.pdf, 2007a.
Osterman G., Bowman K. W., Eldering, A., Fisher, B., et al.: TES Level 2 (L2) Data User's Guide, Version 3.0, Jet Propulsion Laboratory, Pasadena, CA, 40 pp., http://tes.jpl.nasa.gov/uploadedfiles/TES_L2_Data_Users_Guide-1.pdf, 2007b.
Owen, R. C., Cooper, O. R., Stohl, A., and Honrath, R. E.: An analysis of the mechanisms of North American pollutant transport to the central North Atlantic lower free troposphere, J. Geophys. Res., 111, D23S58, doi:10.1029/2006JD007062, 2006.
Parrish, D. D., Holloway, J. S., Trainer, M., et al.: Export of North American ozone pollution to the North Atlantic Ocean, Science, 259, 1436–1439, 1993.
Parrish, D. D., Trainer, M., Holloway, J. S., et al.: Relationships between ozone and carbon monoxide at surface sites in the North Atlantic region, J. Geophys. Res., 103, 13 357–13 376, 1998.
Parrish, D. D., Holloway, J. S., Jakoubek, R., et al.: Mixing of anthropogenic pollution with stratospheric ozone: A case study from the North Atlantic wintertime troposphere, J. Geophys. Res., 105, 24 363–24 374, 2000.
Polvani, L. M. and J. G. Esler: Transport and mixing of chemical air masses in idealized baroclinic life cycles, J. Geophys., Res., 112, D23102, doi:10.1029/2007JD008555, 2007.
Rodgers, C. D.: Inverse Methods for Atmospheric Sounding: Theory and Practice, World Sci., Hackensack, N.J, 2000.
Rodrigues, S., Torres, C., Guerra, J.-C., and Cuevas, E.: Transport pathways of ozone to marine and free-troposphere sites in Tenerife, Canary Islands, Atmos. Environ., 38, 4733–4747, 2004.
Schoeberl, M. R.: Overview of the EOS Aura mission, IEEE Trans. Geosci. Rem. Sens., 44, 5, 1066–1074, 2006.

Shapiro, M. A., Hampel, T., and Krueger, A. J.: The arctic tropopause fold, Mon. Weather Rev., 115, 444–454, 1987.

Shim, C., Li, Q., Luo, M., Kulawik, S., Worden, H., Worden, J., Eldering, A., Diskin, G., Sachse, G., Weinheimer, A., Knapp, D., Montzca, D., and Campos, T.: Characterizing mega-city pollution with TES O_3 and CO measurements, Atmos. Chem. Phys. Discuss., 7, 15 189–15 212, 2007, http://www.atmos-chem-phys-discuss.net/7/15189/2007/.

Singh, H. B., Brune, W. H., Crawford, J. H., Jacob, D. J., and Russell, P. B.: Overview of the summer 2004 International Chemical Transport Experiment- North America (INTEX-A), J. Geophys. Res., 111, D23S02, doi:10.1029/2006JD007905, 2006.

Stohl, A. M. and Trickl, T.: A textbook example of long-range transport: Simultaneos observation of ozone maxima of stratospheric North American origin in the free troposphere over Europe, J. Geophys. Res., 104, 30 445–30 462, 1999.

Stohl, A., Huntrieser, H., Richter, A., Beirle, S., Cooper, O. R., Eckhardt, S., Forster, C., James, P., Spichtinger, N., Wenig, M., Wagner, T., Burrows, J. P., and Platt, U.: Rapid intercontinental air pollution transport associated with a meteorological bomb, Atmos. Chem. Phys., 3, 969–985, 2003, http://www.atmos-chem-phys.net/3/969/2003/.

Stohl, A., Forster, C., Eckhardt, S., et al.: A backward modeling study of intercontinental transport using aircraft measurements, J. Geophys. Res., 108(D12), 4370, doi:10.1029/2002JD002862, 2003b.

Trickl, T., Cooper, O. R., Holger, E., et al.: Intercontinental transport and its influence on the ozone concentrations over Europe: Three case studies, J. Geophys. Res., 108(D12), 8530, doi:10.1029/2002JD002735, 2003.

Worden, H. M., Logan, J. A., Worden, J. R., et al.: Comparisons of Tropospheric Emission Spectrometer (TES) ozone profiles to ozonesondes: Methods and initial results, J. Geophys. Res., 112, D03309, doi:10.1029/2006JD007258, 2007.

Worden, J., Kulawik, S. S., Shephard, M. W., et al.: Predicted errors of Tropospheric Emission Spectrometer nadir retrievals from spectral window selection, J. Geophys. Res., 109, D09308, doi:10.1029/2004JD004522, 2004.

Worden, J., Liu, X., Bowman, K., et al.: Improved tropospheric ozone profile retrievals using OMI and TES radiances, Geophys. Res. Let., 34, L01809, doi:10.1029/2006GL027806, 2007.

Zhang, L., Jacob, D. J., Bowman, K., W., et al.: Ozone-CO correlations determined by the TES satellite instrument in continental outflow regions, and prospects in synoptic climatology, J. Geophys. Res., 33, L18804, doi:10.1029/2006GL026399, 2006.

Zishka, K. M. and Smith, P. J. : The climatology of cyclones and anticyclones over North America and surrounding ocean environs for January and July, 1950–77, Mon. Weather Rev., 108, 387–401, 1980.

Table 1. Map types and meteorological characteristics.

Map Type	2005–2006 Frequency (%)	Characteristics
MAM1	24	Persistent subsiding northwest flow over land areas around back of large semi-stationary low pressure center northeast of Canadian Maritimes, occasional periods of rising motion associated with weak cyclonic disturbances circulating to the south of main circulation center
MAM2	19	Cyclone tracking into northern New England and western Canadian Maritimes possibly accompanied by weak secondary coastal development, areas of rising motion along east coast and offshore in WCB, descending air in DA inland
MAM3	15	Developing coastal cyclone possibly associated with mature cyclone inland, general east-northeast flow along coast with rising motion over the ocean and northern coastal areas; coastal cyclones may be persistent particularly in late spring
MAM4	5	Cyclone well inland producing rising motion in western portion of study domain extending to east coast, offshore general subsiding flow prevails around offshore anticyclone
MAM5	11	Cyclone offshore with frontal system, anticyclone in southeastern Canada, rising motion offshore, light northerly flow and subsidence right along east coast
MAM6	7	Large subtropical anticyclone just off coast and closed low pressure center near Labrador, general subsidence over most of east coast of US and adjacent Atlantic Ocean, strong subsiding northwest flow over Canadian Maritime provinces extending out to sea, light southwesterly flow inland of US east coast

ACPD
8, 19743–19789, 2008

Table 2. O_3-CO slope and correlation (r) for circulation types for Region 1 30–45° N, 75–55° W, Region 2 45–55° N, 65–45° W, and Region 3 30–45° N, 55–40° W.

	Region 1	Region 2	Region 3
All	0.16 (0.32)	−0.03 (−0.06)	0.21 (0.38)
	N=423	N=312	N=317
MAM1	0.14 (0.32)	−0.07 (−0.14)	0.24 (0.42)
	N=101	N=79	N=98
MAM2	0.24 (0.44)	−0.08 (−0.19)	0.28 (0.47)
	N=92	N=74	N=61
MAM3	0.25 (0.42)	0.16 (0.35)	0.29 (0.46)
	N=59	N=32	N=38
MAM4	0.36 (0.53)	0.25 (0.48)	0.28 (0.53)
	N=26	N=25	N=21
MAM5	0.14 (0.32)	−0.10 (−0.14)	0.03 (0.05)
	N=54	N=38	N=38
MAM6	−0.05 (0.05)	−0.14 (−0.34)	0.19 (0.56)
	N=31	N=19	N=17

ACPD
8, 19743–19789, 2008

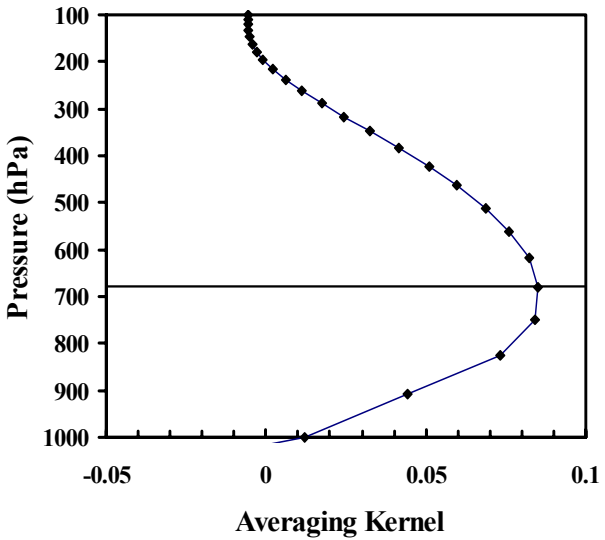

Fig. 1. TES averaging kernel for 681 hPa O_3 for profile near 31° N and 74° W on 6 April 2006. A horizontal line marks the 681 hPa level.

ACPD

8, 19743–19789, 2008

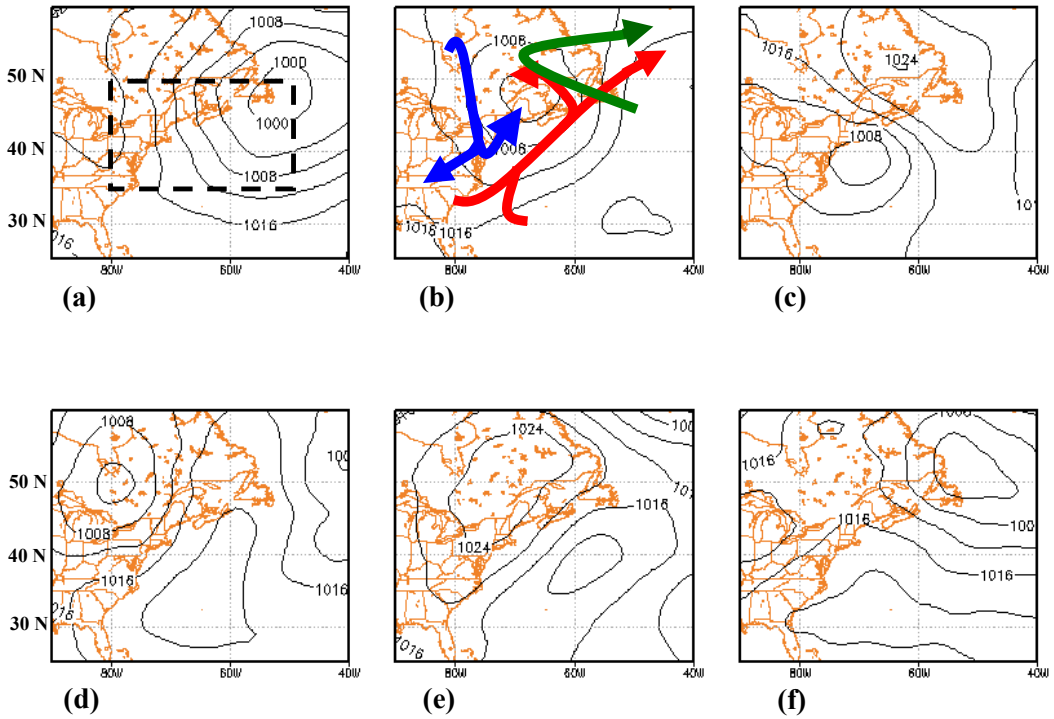

Fig. 2. Composite sea level pressure (hPa) analyses from 2005–2006 for map types MAM1–MAM6 **(a–f)**. The boundaries of the map typing domain are show as dashed lines on a) and schematic representations of the warm conveyor belt (red curve), dry airstream (blue curve) and cold conveyor belt (green curve) are shown on **(b)**.

ACPD

8, 19743–19789, 2008

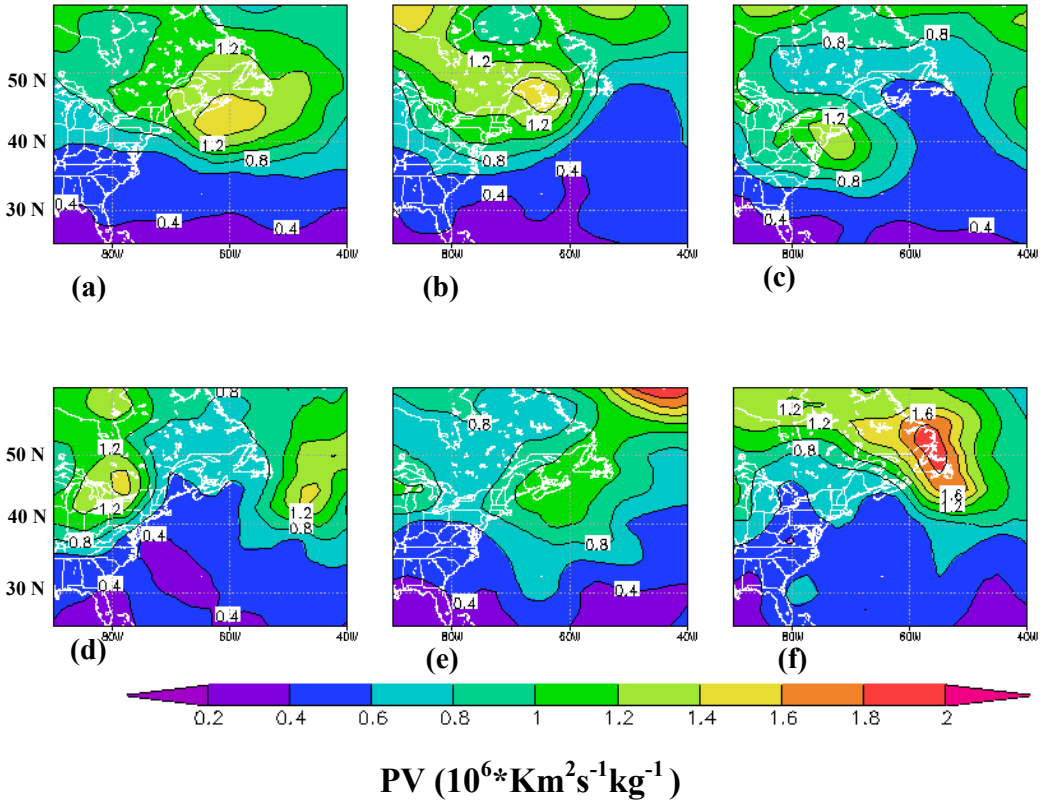

Fig. 3. Mean 400 hPa potential vorticity (PV) for MAM1-MAM6 interpolated from the isentropic surfaces of the NCAR/NCEP Reanalysis **(a–f)**. 1 PVU is 10^6 Km^2 s^{-1} kg^{-1}.

ACPD
8, 19743–19789, 2008

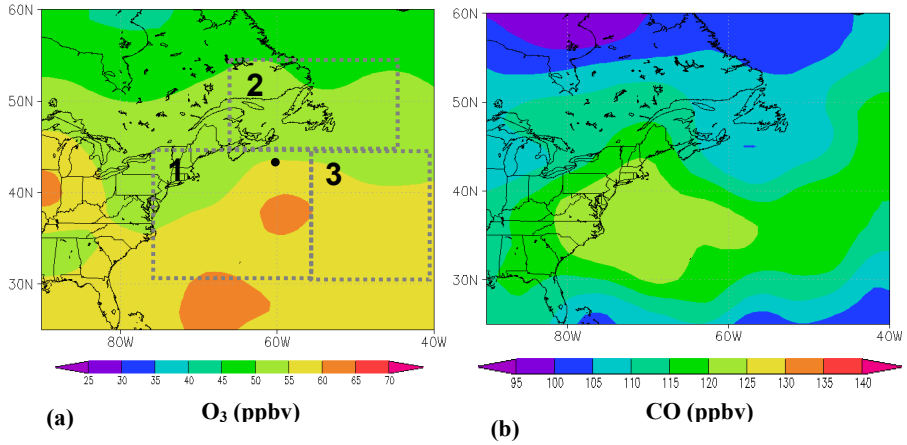

Fig. 4. Spring seasonal composites for 2005–2006 of **(a)** TES 681 hPa O_3 (ppbv) and **(b)** TES 681 hPa CO (ppbv). In (a) the borders of Regions 1, 2, and 3 are shown as dashed lines and the location of Sable Island, NS is shown as a black dot.

ACPD
8, 19743–19789, 2008

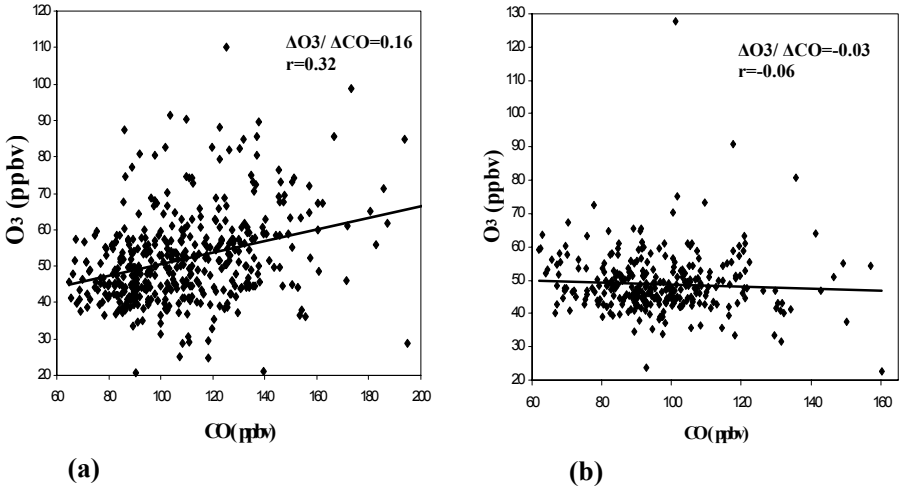

Fig. 5. Scatter plots of TES 681 hPa O_3 versus CO retrievals during MAM 2005–2006 for **(a)** Region 1 and **(b)** Region 2.

ACPD
8, 19743–19789, 2008

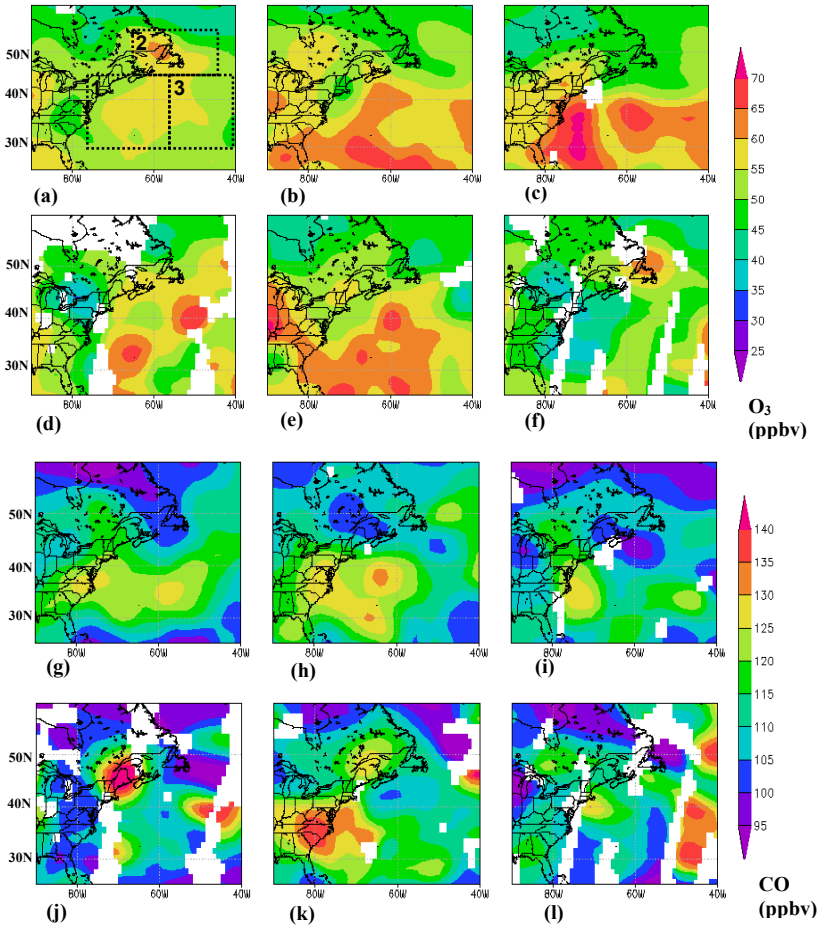

Fig. 6. 681 hPa composites for MAM1 MAM6 for O_3 (ppbv) **(a–f)** and CO (ppbv) **(g–l)**. In (a) the borders of Regions 1, 2, and 3 are shown as dashed lines.

ACPD

8, 19743–19789, 2008

Synoptic influences on North American export observed by TES

J. Hegarty et al.

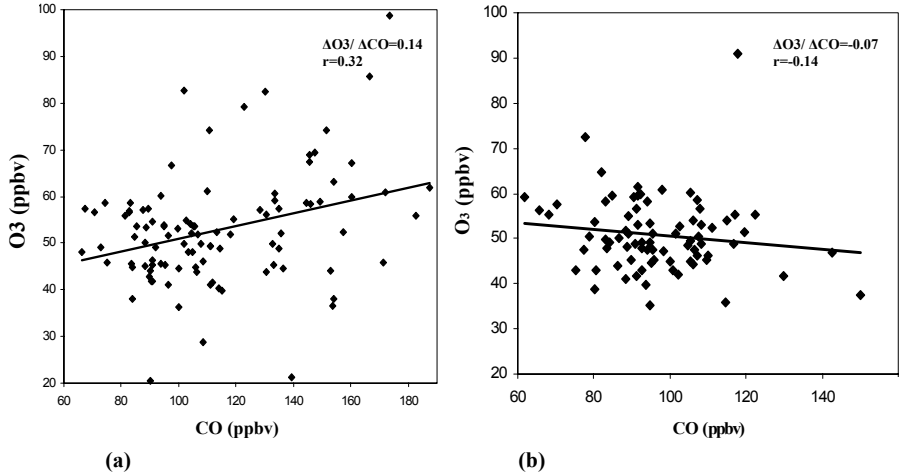

Fig. 7. Scatter plots of TES 681 hPa O_3 versus CO retrievals for MAM1 for **(a)** Region 1 and **(b)** Region 2.

ACPD
8, 19743–19789, 2008

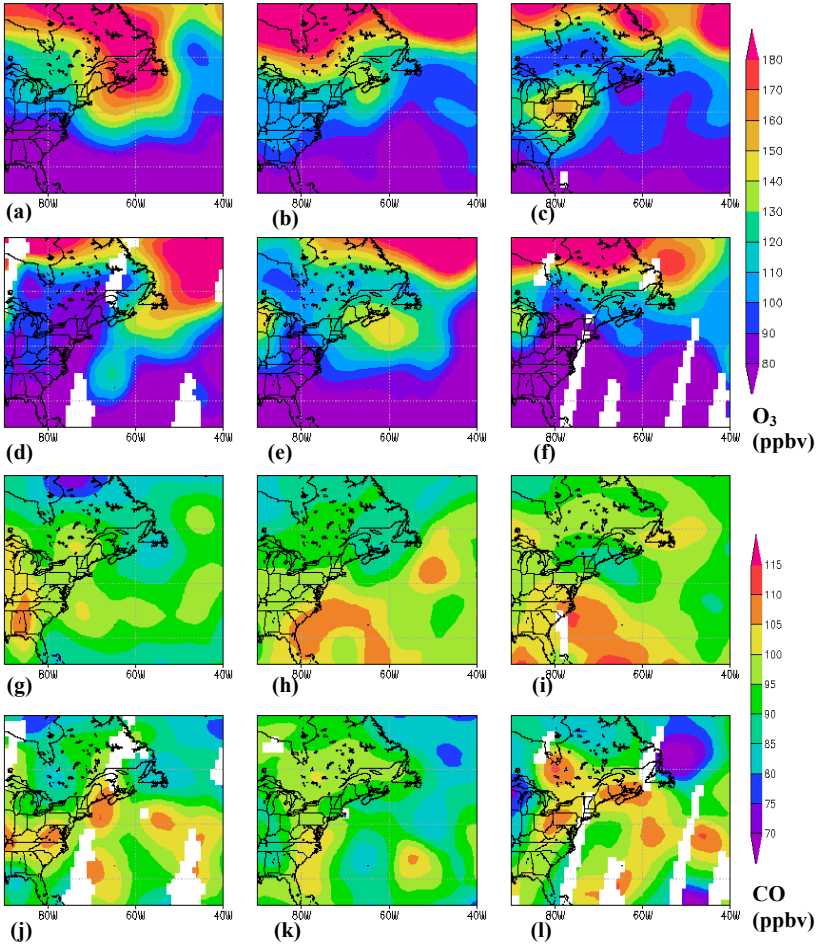

Fig. 8. 316 hPa composites for MAM1 MAM6 for O_3 (ppbv) **((a–f)** and CO (ppbv) **(g–l)**.

ACPD

8, 19743–19789, 2008

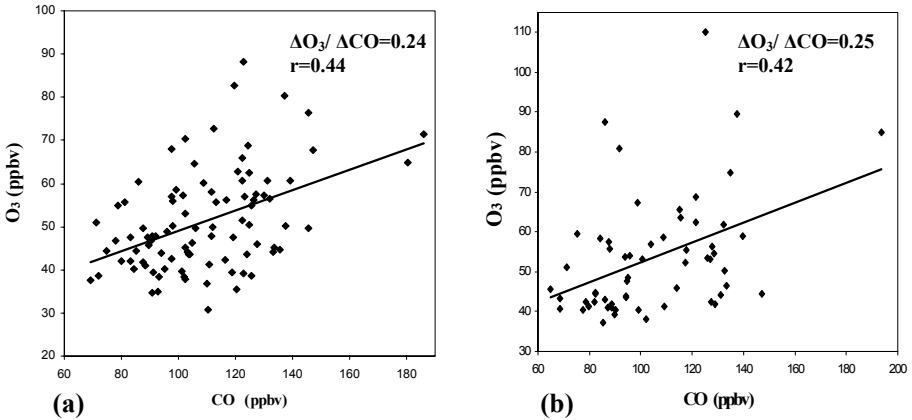

Fig. 9. Scatter plots of TES 681 hPa O_3 versus CO retrievals in Region 1 for **(a)** MAM2 and **(b)** MAM3.

ACPD
8, 19743–19789, 2008

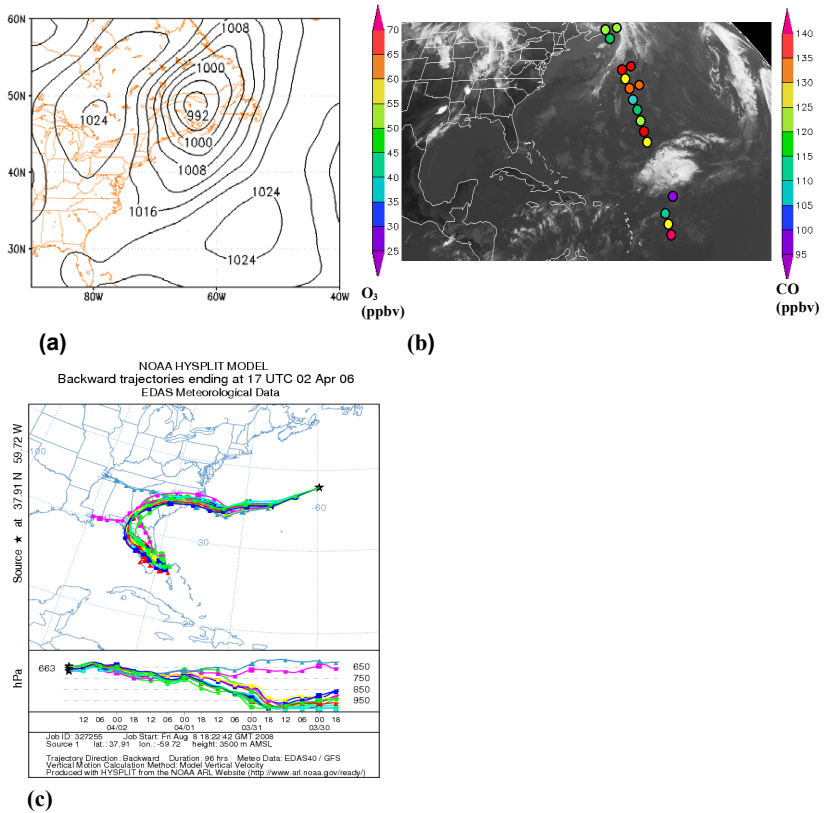

Fig. 10. **(a)** NCEP FNL SLP analysis for 12:00 UTC 2 April 2006 **(b)** GOES East IR image for 17:15 UTC 2 April 2006 with TES 681 hPa O_3 and CO (ppbv) retrievals plotted as colored dots at approximate ground footprint locations. The CO observations are offset slightly to the right from the actual locations and the dot sizes are not representative of the footprint sizes. **(c)** HYSPLIT ensemble back trajectories calculated using EDAS meteorological data for the corresponding time and location of the TES observations from 3500 m above mean sea level.

ACPD
8, 19743–19789, 2008

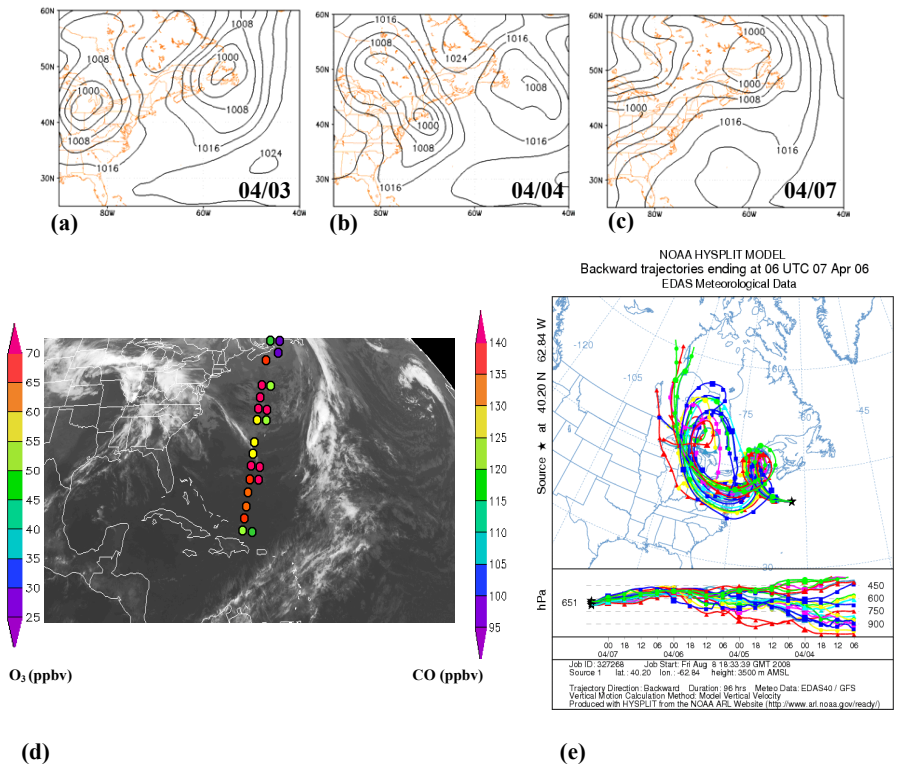

Fig. 11. NCEP FNL SLP analyses (hPa) for 12:00 UTC **(a)** 3 April **(b)** 4 April and **(c)** 7 April 2006 and **(d)** GOES East IR image for 07:15 UTC 7 April 2006 with TES 681 hPa O_3 and CO (ppbv) retrievals plotted for one orbit as colored dots at approximate ground footprint locations. The CO observations are offset slightly to the right from the actual locations and the dot sizes are not representative of the footprint sizes. **(e)** HYSPLIT ensemble back trajectories calculated using EDAS meteorological data for the corresponding time and location of TES observations from 3500 m above mean sea level.

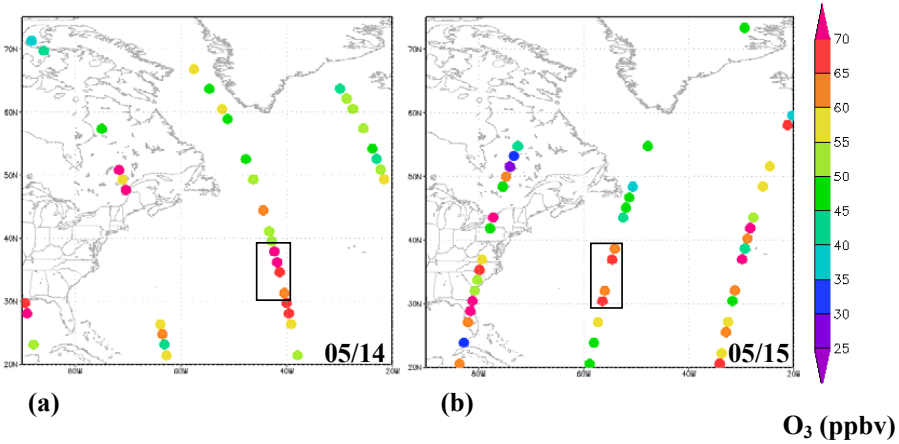

Fig. 12. TES retrievals of 681 hPa O_3 (ppbv) for **(a)** the ascending orbits on the afternoon of 14 May 2006 and **(b)** the descending orbits during the morning of 15 May 2006. The areas of elevated O_3 discussed in the text are enclosed in black rectangles.

ACPD
8, 19743–19789, 2008

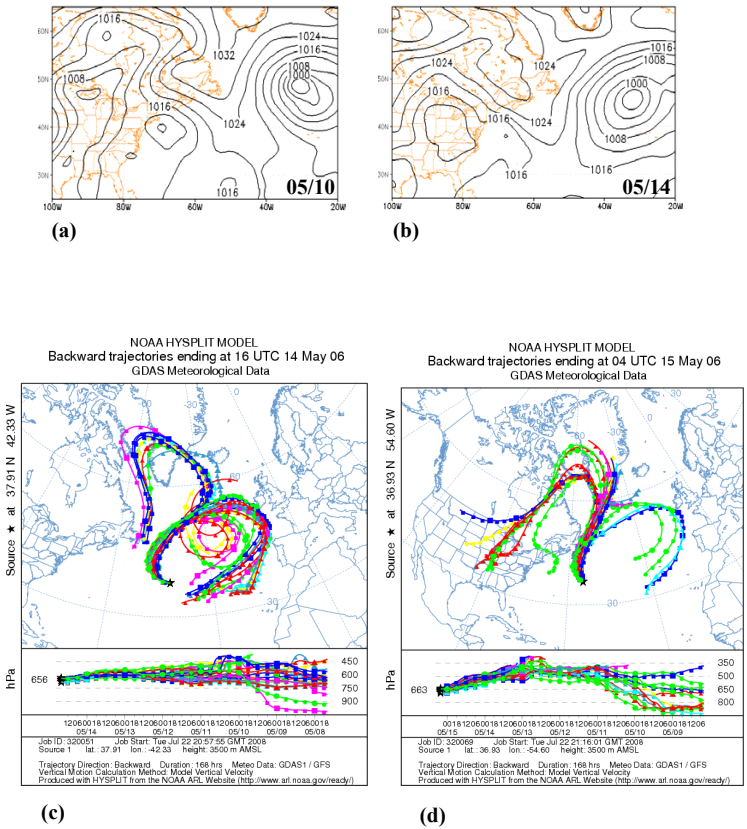

Fig. 13. NCEP FNL SLP (hPa) analyses for 12:00 UTC **(a)** 10 May and **(b)** 14 May 2006. HYSPLIT ensemble back trajectories calculated using GDAS meteorological data starting at **(c)** 16:00 UTC 14 May 2006 from 38°,N and 42° W at 3500 m above mean sea level and **(d)** 04:00 UTC 15 May 2006 from 37° W an 55°,W at 3500 m above mean sea level.

ACPD
8, 19743–19789, 2008